Linking groundwater quality to residence times and regional geology in the St. Lawrence Lowlands, southern Quebec, Canada

Marion SABY[1,*], Marie LAROCQUE[1], Daniele L. PINTI[1, 2],

Florent BARBECOT[1], Yuji SANO[2], Maria Clara CASTRO[3]

1 - GEOTOP and Département des sciences de la Terre et de l'atmosphère, Université du Quebec à Montréal, CP8888 succ. Centre-Ville, Montréal, QC, Canada

2- Atmosphere and Ocean Research Institute, the University of Tokyo, Kashiwa, Chiba 277-8564, Japan

3 - Dept. of Earth and Environmental Sciences, University of Michigan, 1100 N. University, Ann Arbor, MI 48109-1005, USA

* Corresponding author: marion.saby23@gmail.com

Keywords: groundwater quality, groundwater residence times, regional geology, St. Lawrence Lowlands, Quebec (Canada).

ABSTRACT

The assessment of groundwater quality in shallow aquifers is of high societal relevance given that large populations depend directly on these water resources. The purpose of this study was to establish links between groundwater quality, groundwater residence times, and regional geology in the St. Lawrence Lowlands fractured bedrock aquifer. The study focuses on a 4500 km^2 watershed located in the St. Lawrence Lowlands of the province of Quebec in eastern Canada. A total of 150 wells were sampled for major, minor, and trace ions. Tritium (^3H) and its daughter element, ^3He, as well as radiocarbon activity ($A^{14}C$) were measured in a subset of wells to estimate groundwater residence times. Results show that groundwater evolves from a Ca-HCO_3 water type in recharge zones (i.e., the Appalachian piedmont) to a Na-HCO_3 water type downgradient, toward the St. Lawrence River. Locally, barium (Ba), fluoride (F), iron (Fe), and manganese (Mn) concentrations reach 90, 2, 18, and 5.9 mg/L respectively, all exceeding their respective Canadian drinking water limits of 1, 1.5, 0.3, and 0.05 mg/L. Release of these elements into groundwater is mainly controlled by the groundwater redox state and pH conditions, as well as by the geology and the duration of rock-water interactions. This evolution is accompanied by increasing $^3H/^3He$ ages, from 4.78±0.44 years upgradient to more than 60 years downgradient. Discrepancies between calculated $^3H/^3He$ and ^{14}C water ages (the latter ranging from 280 ± 56 to 17,050 ± 3410 years) suggest mixing between modern water and paleo-groundwater infiltrated through subglacial recharge when the Laurentide Ice Sheet covered the study area, and during the following deglaciation period. A linear relationship between ^3H activity and corrected ^{14}C versus Mg/Ca and Ba support a direct link between water residence time and the chemical evolution of these waters. The Ba, F, Fe, and Mn concentrations in

groundwater originate from Paleozoic rocks from both the St. Lawrence Platform and the Appalachian Mountains. These elements have been brought to the surface by rising hydrothermal fluids along regional faults, and trapped in sediment during their deposition and diagenesis due to reactions with highly sulfurous and organic matter-rich water. Large-scale flow of meltwater during subglacial recharge and during the subsequent retreat of the Laurentide Ice Sheet might have contributed to the leaching of these deposits and their enrichment in the present aquifers. This study brings a new and original understanding of the St. Lawrence Lowlands groundwater system within the context of its geological evolution.

1. INTRODUCTION

Anthropogenic activity and climate change are arguably the largest threats to groundwater quality in the 21st century (Aeschbach-Hertig and Gleeson, 2012), however local geology can also have a significant impact (e.g., Nickson et al., 1998; Marimon et al., 2012). Groundwater quality assessment has primarily been carried out using either statistical approaches applied to geochemical data (Li et al. 2012; Mahlknecht et al., 2004; Maclear et al., 2003; Pacheco, 1998; Paralta and Ribeiro, 2001), geochemical modeling (Carrillo-Rivera et al., 2002; Homoncik et al., 2010; Marimon et al., 2012), or by tracing groundwater flow using stable and radioactive isotopes (Clark and Fritz, 1997; Barbecot et al., 2000). These approaches require an understanding of the present geological context, but not of the geological evolution of the region. However, knowledge of the geological evolution of a particular region might prove critical to understand which individual element or set of elements are present and how they interact with each other and with the host media, in addition to their spatial distribution in a particular area. Very few studies consider the diverse relationships between the past and present hydrogeological contexts and the geological evolution of the studied area, the groundwater residence time, the occurrence of highly mineralized fluids, and their role in the formation of economic deposits (e.g., Aquilina and De Dreuzy, 2011a; Kloppmann et al., 2002).

With more than five million inhabitants, the St. Lawrence Lowlands is the most densely populated region in the Canadian province of Quebec. This region hosts most of the agricultural and industrial activities of the province. Approximately 5% of the groundwater extracted in this area is used as drinking water (MDDELCC, 2012). The region is characterized by a regional

fractured bedrock aquifer of Cambro-Ordovician age, overlain by discontinuous and often perched Quaternary granular aquifers. Several studies carried out in southern Quebec have highlighted the presence of high barium (Ba), fluorine (F), iron (Fe), and manganese (Mn) concentrations (Lacasse, 2013) in fresh and brackish groundwater (Cloutier et al., 2010). High concentrations of these elements have been observed in the Becancour (Meyzonnat et al., 2015) and Eastern Monteregie (Beaudry, 2013) watersheds in particular, but their origins (i.e., anthropogenic or natural) and release mechanisms into groundwater are not yet fully understood.

The purpose of this study was to establish links between groundwater quality, groundwater residence times, and regional geology in the St. Lawrence Lowlands fractured bedrock aquifer. This study focused on the Nicolet-St. François watershed (henceforth referred to as NSF), which is located between the previously mentioned Becancour and Eastern Monteregie watersheds (Fig. 1). Understanding the regional geology and the emplacement of geological units over time is extremely important to understanding past fluid circulation and the impact of these mineralized fluids and rocks on the current groundwater chemical signature. Here, groundwater contains relatively high levels of F, Ba, Mn, and Fe. To understand the spatial distributions of these ions and their origins in groundwater, the groundwater chemistry and regional flow were traced using major and trace elements measured in 150 wells, and residence times were estimated with the $^{3}H/^{3}He$ and ^{14}C methods in a few select wells. Geochemical analyses were also made on rock cuttings to constrain concentrations of anomalous elements in the bedrock aquifer. These were compared with the corresponding concentrations in the groundwater.

2. GEOLOGY AND HYDROGEOLOGY OF THE STUDY AREA

2.1 Geology

The study area corresponds to the Nicolet River Basin and the lower part of the Saint-François River watershed, in the Centre-du-Québec region (Fig.1a). The regional fractured aquifer is composed of rocks belonging to two geological provinces: the Appalachian Mountains in the southeastern part of the basin, and the St. Lawrence Platform in the northwestern part (Fig. 1a). Geographically, the area is part of the St. Lawrence Lowlands.

The St. Lawrence Platform is a Cambrian-Lower Ordovician siliciclastic and carbonate platform, formed in an extensional context related to the opening of the Iapetus Ocean, and overlain by Middle-Late Ordovician foreland carbonate-clastic deposits, which were deposited during the closure of Iapetus and the Appalachian Mountains buildup. Cambrian Potsdam Group quarztitic sandstone, Early Ordovician dolostone of the Beekmantown and Chazy Groups, Middle-Late Ordovician carbonates of the Black River and Trenton Groups, carbonate-rich Utica shale and the silty-shale of the Lorraine/Sainte-Rosalie Groups, and molassic shales of the Queenston Group are unconformably deposited on the gneiss granite anorthosite terrains of the Proterozoic Grenville Province (Globensky, 1987). Cambrian green and red shales of the Sillery Group, slate, limestone, and sandstone conglomerate of the Bourret Fm, schists of the Drummondville Olistostrome, calcareous slate of the Bulstrode and Melbourne Fm, and schists, shales, sandstone and conglomerates of the Shefford, Oak Hill, and Sutton-Bennett Groups outcrop in the Appalachian piedmont (Globensky, 1993).

Unconsolidated Quaternary fluvio-glacial deposits cover the fractured Paleozoic aquifer (Lamothe, 1989). Basal deposits are tills from the last two Quaternary deglaciation episodes (45 and 13 ka BP), followed by glacio-lacustrine sandy and organic deposits. A thick clay layer deposited during the Champlain Sea episode (12-9 ka BP; Bolduc and Ross, 2001) covers sandy deposits over a 30 km strip along the St. Lawrence River (Lamothe and St-Jacques, 2014). This thick clay layer led to the confinement of the underlying fractured bedrock aquifer and Quaternary deposit aquifers in this narrow area. Further upgradient, the clay layer is no longer uniform, creating a flat area composed of sand, patches of clay, and shale, which led to a heterogeneous and semi-confined hydrogeological context. Upgradient, reworked till and bedrock outcrops leave the fractured aquifer unconfined in its main recharge zone (Fig. 1b).

2.2. Hydrogeology

The study area is divided into two main aquifer systems (Larocque et al., 2015). The first corresponds to superficial unconsolidated Quaternary aquifers of relatively limited thickness (1 to 80 m), and the second system is the underlying Paleozoic fractured bedrock aquifer. Hydraulic conductivities in the fractured bedrock aquifer are heterogeneous and range from 5×10^{-9} m/s to 7×10^{-6} m/s (Larocque et al., 2015). Hydraulic conductivities in the Quaternary units range from 1.2×10^{-5} m/s for sand to 5.8×10^{-7} m/s for till. Groundwater flows from recharge zones in the Appalachian piedmont toward the St. Lawrence River, and the main tributaries, the Nicolet and Saint-François rivers. The mean depth of the water table is 4.4 m. The annual volume of abstracted groundwater is 23.4 Mm^3, corresponding to 3% of the annual recharge (152 mm; Larocque et al., 2015). Most of the study area is either cultivated (48%, mainly along the

St. Lawrence River) or forested (45%, mainly in the Appalachian piedmont) (Larocque et al., 2015). Urbanized zones, surface water, and wetlands occupy 2, 1.1, and 3.7% of the study area respectively. Agriculture is dominated by corn (27%), hay (22.4%), and soybean (19.8%) production (Larocque et al., 2015). The 1961-2010 average annual temperature for the study area is 5.6°C, and the average annual precipitation is 1018 mm/yr (25% as snowfall; Nicolet and Drummondville stations, Environment Canada, 2014).

3. SAMPLING AND ANALYTICAL METHODS

Between June and August 2013, 150 groundwater samples (147 in the fractured bedrock aquifer, and 3 in the granular deposits; designated by NSF in Tables 1 and A1) were collected from private and municipal open bedrock wells with depths ranging between 1 and 250 m (Fig. 2). Ten additional observation wells and five piezometers were drilled and instrumented as part of this project (designated by NSF-R in Tables 1 and A1). The five piezometers are 2.5 cm in diameter, have a 1 m screen at their lower end, and reach between 2 and 10 m depth. The ten drilled bedrock wells and all the other private bedrock wells are cased along the section crossing the unconsolidated Quaternary deposits and are open in the bedrock aquifer (depths ranging between 52 and 91 m). Domestic and observation wells were purged of a volume equivalent to three times the borehole volume (GRIES, 2011) and water was sampled once its chemo-physical parameters had stabilized (pH, temperature, redox potential, and electric conductivity, measured with an air-tight cell). Continuously pumped municipal wells were sampled directly. Groundwater was collected at the observation wells using a submersible pump with speed control

(Redi-Flo2®), maintaining the whole sampling line under pressure to prevent water degassing. All samples were filtered to 0.45 μm in the field and analyzed for chemo-physical parameters *in situ*. A subset of twenty samples was also analyzed for ^{3}H and helium isotopic ratios ($^{3}He/^{4}He$). Ten of these were also analyzed for ^{14}C and $\delta^{13}C$ of the total dissolved inorganic carbon (TDIC). This last subset of samples was selected such that the wells would be representative of the general flow gradient, spanning the Appalachian recharge zone to the St. Lawrence River. A further 14 water samples (Fig. 2) were collected for noble gas analysis using 3/8 inch refrigeration-type copper tubes (Weiss, 1968). Water was allowed to flow for several minutes prior to sealing the copper tubes with stainless steel clamps. All water samples were kept at 4°C during storage and transport. Rock samples were taken from drilling wastes of the seven bedrock wells drilled during the study in order to quantify the amount and distribution of different elements found in excess of drinking water limits in the aquifer material. These samples have been selected to follow the regional groundwater flow path, from the recharge zone to the discharge zone (cf. Fig. 2).

A certified laboratory (ISO/CEI 17025) analyzed major, minor (±0.5%) and trace (±2%) solute ions and alkalinity using the ICP-MS method for ion analysis and titration at pH 4.5 for alkalinity. HCO_3 was computed from alkalinity using Diagramme® software (available at http://www.lha.univ-avignon.fr/LHA-Logiciels.htm). Helium isotopes were analyzed at the Noble Gas Laboratory of the University of Michigan and at the Atmospheric and Ocean Research Institute (AORI) of the University of Tokyo. At the Noble Gas Laboratory of the University of Michigan, noble gas isotopes were measured on a MAP-215 mass spectrometer. Elemental abundances of He and Ne are associated with uncertainties of 1.5 and 1.3% respectively, at ± 1σ

level. Details on the noble gas analytical procedure of the University of Michigan can be found in Ma et al. (2005) and Castro et al. (2009). Samples analyzed at AORI of the University of Tokyo were degassed offline and subsequently purified in a line connected to a Helix SFT. Helium isotopes were analyzed and compared to the Helium Standard of Japan (HESJ) standard (Matsuda et al., 2002), with a 2σ precision of ±0.2% (Sano et al., 2008). ^{4}He and ^{20}Ne concentrations were measured on a Pfeiffer QMS Prisma^{TM} connected to the purification line. Details on the analytical procedure of the University of Tokyo can be found in Sano et al. (2008). Tritium was analyzed at the Environmental Isotope Laboratory (EIL) of the University of Waterloo using liquid scintillation counting (LSC). Samples analyzed for tritium were concentrated 15 times by electrolysis prior to counting. The detection limit for enriched samples is 0.8 TU (Heemskerk and Johnson, 1998). Groundwater for $^{3}H/^{3}He$ and ^{14}C age determination was sampled from wells along what was expected to be the main groundwater flow directions (Fig. 2; Table 1).^{14}C activity and $\delta^{13}C$ in groundwater were analyzed at the Beta Analytic Inc. Laboratory, Florida, using a Single Stage Accelerator Mass Spectrometer (SSAMS). ^{14}C measured activity ($A^{14}C$) was expressed in percent of modern carbon (pMC). The ^{13}C content of TDIC is reported using δ (‰) notation, as a deviation from the Vienna-Belemnite from the Pee Dee formation (V-PDB, North Carolina, USA).

Seven rock samples were analyzed for whole rock geochemistry (Fig. 2; Table 2) at ACME Lab in Vancouver. The samples were crushed to 80% passing 10 mesh (2 mm) and pulverized to 85% passing 200 mesh (75 μm). The powders were mixed with $LiBO_2/Li_2B_4O_7$ flux in the laboratory, fused, and dissolved in ACS-grade nitric acid, and analyzed by ICP for major

195 elements and ICP-MS for minor elements. Total carbon and sulfur were measured using the Leco
196 method (LECO Corporation, 2007).

197

198 **4. RESULTS**

199 Table A1 (in the Appendix) reports the main physico-chemical parameters of the 150
200 sampled wells measured in the field, together with the major ion concentrations, and those of Ba,
201 F, Fe, Mn, and Sr. Table 1 shows the tritiogenic ^3He concentrations ($^3He_{tri}$ in cm^3STP/g_{H2O}) and
202 tritium (^3H in TU), used for calculating $^3H/^3He$ ages in the selected wells. The measured ^{14}C
203 activities ($A^{14}C$ in pMC) and the $\delta^{13}C$ of soil CO_2 are also reported as uncorrected ^{14}C ages (A_0 =
204 100 pMC) and corrected ^{14}C ages, using the Fontes and Granier equilibrium model (henceforth
205 the F&G equil; Fontes, 1992). Uncertainties on the ^{14}C uncorrected ages are estimated to be
206 ±0.5% of the reported value, and are related to the analytical uncertainties of the measured $A^{14}C$
207 (Table 2). Uncertainties of ±20% of the reported value for the corrected ^{14}C ages depend
208 essentially on the assumed $\delta^{13}C$ of the soil CO_2 for the F&G equil (see section 4.2 for details).

209 Table 2 reports major oxides and trace elements of the rock cuttings. Table 3 reports the
210 results of a Hierachical Cluster Analysis (HCA) applied to all 150 samples, performed using the
211 commercial software package JUMP®. This HCA highlights the statistical robustness of the
212 relationship between water chemistry types (determined based on the major ions) and the relative
213 enrichments of trace ions in groundwater.

214

4.1 Groundwater chemistry

92.5% of all water samples from the current study are of Ca,Mg-HCO_3 and Na-HCO_3 type (Fig. 3). The Ca,Mg-HCO_3 type represents modern freshwater, where the dissolution of Quaternary calcareous tills and Ordovician calcareous shales of the fractured aquifer is the dominant process (Cloutier et al., 2010; Meyzonnat et al., 2015). This water circulates mainly in the unconfined aquifers of the Appalachian piedmont (Fig. 2). The Na-HCO_3 group represents more evolved groundwater, the chemistry of which is mainly controlled by Ca^{2+}–Na^{+} ion exchange, whereby Ca^{2+}_{water} exchanges with $Na^{+}_{mineral}$ (e.g., Cloutier et al., 2010). This water type occurs downgradient in the study area, both in semi-confined and confined environments. A few water samples close to the St. Lawrence River are of Na-Cl, Na-SO_4, and Ca-Cl water types (Fig. 3). The Na-Cl water type represents groundwater with salinity derived from mixing with pore seawater trapped in the Champlain Sea clays or in the fractured rock aquifers (Meyzonnat et al., 2015). Two samples, NSF-R7 and NSF165 (Table A1), located upgradient in the study area, have abnormally high NaCl concentrations, of 3500 and 260 mg/L respectively. Such high Na/Cl ratios are likely the result of local pollution from road deicing salt.

Plots of Mg/Ca ratios versus pH can provide information on carbonate dissolution processes (Cloutier et al., 2010). A Mg/Ca ratio of between 0.5 and 1 is representative of young, Ca,Mg-HCO_3 type groundwater in equilibrium with calcite and dolomite. In the study area, this diagram shows a positive trend between Mg/Ca and pH, suggesting incongruent-dissolution of Mg-calcite or dolomite along the regional flow path (Fig. 4a), and is concordant with the geochemical downgradient groundwater evolution. A plot of (Ca+Mg)/(Na+K) ratios versus total

236 cations (Fig. 4b) suggests cationic exchange between Ca and Na (Appelo and Postma, 2005;
237 Cloutier et al., 2006). Calcium derived from Ca-HCO_3 type water replaces the sodium from clay
238 or iron minerals. This process enriches the water in Na^+ compared to Ca^{2+}, confirming the ion
239 exchange. A similar process depletes Ca^{2+} from downgradient groundwater. A saline water end-
240 member is identified by the shift of the Na-Cl and Na-SO_4 water groups. This shift is thought to
241 indicate mixing between fresh and saline water (Fig. 4b).

242 Ten wells show Ba concentrations above the drinking water threshold value of 1 mg/L
243 (Table A1), and twelve wells show Ba concentrations of between 0.5 and 1 mg/L. F exceedances
244 are rare in the study area, with only two wells exceeding the drinking water quality standard of
245 1.5 mg/L (Health Canada, 2014), and eight wells with concentrations of between 1 and 1.5 mg/L
246 (Table A1). Fe concentrations are as high as 18 mg/L in 32 wells, compared with the Canadian
247 esthetic quality standard of 0.3 mg/L (Health Canada, 2014), and Mn concentrations are as high
248 as 5.9 mg/L, compared with the Canadian esthetic quality standard of 0.05 mg/L (Health Canada,
249 2014; Table A1).

250 Rock analyses from seven locations (Fig. 2) show that Ba concentrations range from 124
251 to 1055 ppm, F concentrations from 386 to 955 ppm, and Fe_2O_3 concentrations from 1.27 to
252 8.55%. MnO concentrations vary between 0.03 and 0.18% in both the St. Lawrence Lowlands
253 and the Appalachian Mountains (Table 2). Other analyses performed as part of previous studies
254 in the area show even higher maximum values: greater than 1500 ppm Ba and F, greater than
255 20% Fe_2O_3, and greater than 0.25% MnO (SIGEOM, 2014).

256

4.2. $^{3}H/^{3}He$ and ^{14}C groundwater residence times

The calculation of $^{3}H/^{3}He$ ages requires the separation of helium derived from the decay of post-bomb tritium ($^{3}He_{tri}$) from all other helium components potentially present in groundwater. These additional components may include 1) atmospheric helium in solubility equilibrium with water (He_{eq}), 2) excess air helium (He_{ea}), which results from air bubbles entering the water table, and 3) terrigenic helium (He_{terr}), produced by U and Th decay in the crust and/or derived from a mantle component. The Weise-plot diagram (Fig. 5) shows helium isotopic ratios, for which both numerator and denominator have been corrected for air contamination by substracting the ^{3}He and the ^{4}He amounts derived from excess air (ea)) ($^{3}He_{tot}$-$^{3}He_{ea}$)/($^{4}He_{tot}$-$^{4}He_{ea}$). The corrected excess air $^{3}He/^{4}He$ ration (here normalized to the $^{3}He/^{4}He$ ratio in the atmosphere Ra = 1.386 x 10^{-6}, is plotted against the inverse of the normalized helium concentration corrected for excess-air ($^{4}He_{eq}$/($^{4}He_{tot}$-$^{4}He_{ea}$)) (Weise and Moser, 1987). Mixing between the different end-members is represented by a linear equation, Y= mX+b (Weise and Moser, 1987), as per eqn. 1:

$$\underbrace{\frac{\left({}^{3}He_{tot}-{}^{3}He_{ea}\right)}{\left({}^{4}He_{tot}-{}^{4}He_{ea}\right)}}_{Y}=\underbrace{\left(R_{eq}-\mathrm{R}_{terr}+\frac{{}^{3}He_{tri}}{{}^{4}He_{eq}}\right)}_{m}\cdot\underbrace{\frac{{}^{4}He_{eq}}{{}^{4}He_{tot}-{}^{4}He_{ea}}}_{X}+\underbrace{R_{terr}}_{b} \qquad (1)$$

where He_{tot} is the total measured helium, R_{eq} is the $^{3}He/^{4}He$ ratio of the atmospheric helium in solubility equilibrium with water (0.984 Ra; Benson and Krause, 1980), and R_{terr} corresponds to the time-integrated ratio of ^{3}He and ^{4}He radiogenic production of the crust and/or mantle He addition. Straight lines traced along groups of samples represent mixing of post-bomb

276 groundwater accumulating $^{3}He_{tri}$ and pre-bomb radiogenic ^{4}He enriched groundwater (Fig. 5).
277 The slope, "m", of eqn. (1) is associated with the amount of tritium that completely decayed into
278 $^{3}He_{tri}$ and the Y-intercept, R_{terr} (the "b" term in eqn. 1). Groundwater helium can be explained by
279 the decay of 4 to 67 TU of tritium mixed with terrigenic helium characterized by R_{terr} ranging
280 from 0.05 to 0.70Ra. This R_{terr} value is higher than that expected for local production from Li
281 (^{3}He), U and Th (^{4}He) present in local formations (0.012Ra; Pinti et al., 2011; Méjean et al.,
282 2015) and suggests a mantle helium contribution on the order of 0.5 to 8.6%. This mantle helium
283 is derived from the leaching of plutonic intrusions of the Cretaceous Monteregian Hills (Pinti et
284 al., 2011). $^{3}He_{tri}$ can be estimated following the equation of Schlosser et al., 1989:

285 $$^{3}He_{trit} = {}^{4}He_{tot} \cdot (R_{tot} - R_{terr}) - {}^{4}He_{eq} \cdot (R_{eq} - R_{terr}) - \left(\frac{^{4}He}{^{20}Ne}\right)_{ea} \cdot (^{20}Ne_{tot} - {}^{20}Ne_{eq}) \cdot (R_{ea} - R_{terr}) \quad (2)$$

286 where R is the measured $^{3}He/^{4}He$ ratio in groundwater; R_{atm} and $(^{4}He/^{20}Ne)_{ea}$ are generally
287 assumed to be atmospheric (R_{atm} = 1.382 x 10^{-6}; Sano and Fischer, 2013; $[^{4}He/^{20}Ne]_{exc}$ = 0.3185;
288 Ozima and Podosek, 1983). Measured tritium in the current study ranges from the detection limit
289 value of 0.8 TU (NSF224 and NSF-R1) to 12.7 TU (NSF219) (Table 1).

290 Calculated $^{3}H/^{3}He$ ages vary between 4.8±0.4 years in well NSF215, upgradient, and
291 60.0±3.2 years in well NSF-R4, downgradient, in the fractured bedrock aquifer (Table 1; Fig. 2).
292 $^{3}H/^{3}He$ ages cannot be calculated for sample NSF-R1, located downgradient. The tritium content
293 for this well is below the detection limit of 0.8 TU, indicating that water recharged prior to the
294 bomb peak (background ^{3}H of 5-6 TU; Clark and Fritz, 1997) and that any detectable tritium has
295 completely decayed since then. This sample also contains very high amounts of radiogenic ^{4}He,

296 5.29 x 10^{-6} cm^3STP/g_{H2O}, two orders of magnitude higher than the atmospheric amount of helium
297 in solubility equilibrium with water (Air saturated Value or ASW; i.e. 4.6 x 10^{-8} cm^3STP/g_{H2O} at
298 10˚C; Smith and Kennedy, 1983). This high amount of radiogenic ^4He indicates the presence of
299 paleo- water, possibly tens of thousands of years old, as also indicated by uncorrected ^{14}C ages
300 (see below). Calculated $^3H/^3He$ ages for samples NSF137, 149, 150, 221 and 224 (Table 1) are
301 older than 60 years, and are therefore at the limit of the dating method. This is due to the fact that
302 their measured $^3He/^4He$ ratios are very radiogenic, i.e. close to the R_{terr} end-member(Fig. 5). The
303 calculation of $^3He_{tri}$ can be difficult to assess because it is overshadowed by the $^3He_{terr}$ and this
304 can easily lead to an under- or overestimation of the $^3He_{tri}$ and so of the ages.

305 Measured ^{14}C activities ($A^{14}C$) plotted against the $\delta^{13}C$ of TDIC generally show an
306 inverse trend ($R^2 = 0.74$), suggesting the evolution of groundwater carbon content with age (Fig.
307 6a). Post-bomb tritium-rich groundwater dissolves biogenic soil CO_2 ($A^{14}C$ = 120 pMC; $\delta^{13}C \sim$ -
308 23‰), evolving with time and accumulating dead carbon from carbonate dissolution ($A^{14}C$ = 0
309 pMC; $\delta^{13}C$ = 0‰; sample NSF-R1). Uncorrected ^{14}C ages range from 230 ± 56 years for well
310 NSF219, located in the main recharge area of the Appalachians piedmont, to 17,050 ± 3410 years
311 for well NSF-R1, located downgradient in a semi-confined zone (Table 1; Fig. 2). ^{14}C activities
312 were corrected for carbonate dissolution ($A_0{}^{14}C$) using the F&G equil model (Fontes, 1992). This
313 is the only ^{14}C age model adapted to carbonate-dominated aquifers which takes into account both
314 the dissolution of carbonates and the Ca-Na exchange processes (Fontes, 1992; Plummer and
315 Glynn, 2013). Corrected ^{14}C ages range from 280 ± 2 yrs for well NSF219 to 10,210 ± 80 years
316 for well NSF221 which is located in the plain at the base of the Appalachian piedmont, in a semi-
317 confined aquifer (Fig. 2). The F&G equil model fails to provide a corrected ^{14}C age for well

318 NSF-R1, probably because of its high levels of dead carbon ($A^{14}C$ = 6.5 pMC and $\delta^{13}C$ = 1.9 ‰).
319 Other well-known ^{14}C correction models of Pearson (1992), Mook (1972), IAEA (Salem et al.,
320 1980), Evans et al. (1979), and Eichinger (1983) are not able to calculate a ^{14}C age for NSF-R1
321 groundwater. Only ^{14}C activities corrected with the model of Tamers (1967) allow the calculation
322 of a corrected ^{14}C age, of 17,050±3410 years (Table 1).

323 The apparent contradiction between calculated $^{3}H/^{3}He$ and ^{14}C ages (Table 1) is often
324 observed in aquifers (i.e., Andrews, 1985; Patriarche et al, 2004; Castro and Goblet, 2005) and is
325 thought to result from the mixing of water masses having different ages and origins. This is
326 apparent from the significant relationship (R^2 = 0.80) between measured ^{14}C and ^{3}H activities
327 (Fig. 6b). Samples from the current study area (NSF) have been compared to those from the
328 neighboring Becancour watershed (BEC; data from Vautour et al., 2015) to show that such
329 mixing is a common occurrence and dominant process in the St. Lawrence Lowlands aquifers.
330 The first end-member represents recently recharged freshwater containing some post-bomb ^{14}C
331 ($A^{14}C$ = 97.3 pMC) and tritium (^{3}H = 12.7 TU). The second end-member is an older
332 groundwater, recharged prior to 1952, and thus containing pre-bomb tritium (< 0.8 TU; Clark and
333 Fritz, 1997) as well as $A^{14}C \leq 6.5$ pMC, the latter derived by the addition of dead carbon from the
334 carbonate pool. Most modern water (well NSF219) is of Ca-HCO_3 type at a depth of 6.1 m, while
335 the oldest water (well NSF-R1) is of Na-Cl type under entirely confined conditions at a depth of
336 84.4 m. This mixing could have taken place in the wells or in the aquifer itself. The first
337 hypothesis is unlikely, because the totality of the sampled wells from the fractured aquifer are
338 equipped with casing that prevents water from the unconsolidated granular aquifer to flow into

339 the fractured one. Thus the observed mixing between freshwater and fossil water is expected to
340 have occurred in the fractured aquifer itself.

341

342 **5. DISCUSSION**

343 *5.1 Trace elements and groundwater quality*

344 HCA applied to the major and trace ions of the 150 sampled wells (Table 3) allows the
345 relationship between the chemical evolution of groundwater in the watershed and their trace
346 element concentrations, such as those of Ba, F, Fe, and Mn, to be highlighted. The HCA indicates
347 that the more evolved waters are those enriched in Ba, F, Fe, and Mn. These are 1) Ca-HCO_3
348 groundwater, mainly located downgradient, far from the main recharge zone of the Appalachian
349 Mountains, and in a semi-confined environment; 2) evolved Na-HCO_3 waters which underwent
350 Ca-Na ionic exchange (Table 3).

351 Calculated ^{14}C ages support the occurrence of prolonged water-rock interactions, which
352 could have led to the release of trace elements such as Ba, F, Fe, and Mn into groundwater. This
353 water evolved chemically with time, as shown by the Mg/Ca ratio, which inversely correlates
354 with ^{3}H activities (Fig. 7a) and positively correlates with corrected ^{14}C ages (Fig. 7b). It is also
355 apparent that water types tend to follow this pattern by evolving downgradient from Ca-HCO_3 to
356 Na-HCO_3 (Fig. 7b).

357 Ba concentrations tend to increase from upgradient to downgradient along the general
358 flow path (Fig. 8). Ba increases significantly when water flows through the Sillery group, the

Bourret Fm and the Olistotrome of Drummondville, which correspond to the same type of rocks as those which host barium economic deposits (see Fig. 8 and section 5.2). A second increase in Ba occurs in the Lorraine and Ste-Rosalie Groups. Concentrations finally decrease in the Queenston Group.

Fluorine has been reported as problematic in other basins of the St. Lawrence Lowlands, particularly in the Eastern Monteregie (Beaudry, 2013). Plotting Ca versus F concentrations (Fig. 9a) yields a saturation curve which highlights the precipitation of calcium-fluorine by groundwater circulation as a result of the release of F into groundwater. However, results also show a clear relationship between pH and F in groundwater (Fig. 9b), which can signify an exchange between F^- and OH^-, a process called desorption (Savenko, 2001). Desorption of F tends to occur above a pH of 7 (Hounslow, 1995), increasing with pH and OH^- availability.

Fe and Mn sources in groundwater are known to be related to pH and redox conditions (Homoncik et al., 2010). Figure 10a shows that Fe^{2+} and Mn^{2+} can be mobilized in groundwater over a large range of pH and Eh values. Generally, Fe is more soluble under the Fe^{2+} form in weakly oxidizing water and reducing water than Mn. Mn will be more soluble under the Mn^{2+} form in more strongly oxidizing water. Some samples have very low Fe and Mn concentrations despite the fact that conditions are favorable for their release into groundwater, implying that these elements are not fully available in the matrix. Reducing water conditions seem to better explain Fe availability in water than does pH (Fig. 10a). For Mn, the relationship with Eh and pH is less clear than for Fe, but reducing water is still the main factor controlling the concentration of

379 dissolved Mn in groundwater. In near-neutral pH conditions, interactions between Fe and Mn can
380 occur (Collins and Buol, 1970).

381 The scatterplot of Fe versus Mn (Fig. 10b) shows that high Fe concentrations are found
382 only with high Mn concentrations, while high Mn concentrations can occur in the presence of a
383 wide range of Fe concentrations, probably because of its greater availability in the host rock. The
384 high affinity of Mn to ferric oxides could lead to its removal by occlusion and sorption to
385 precipitated Fe (Morgan and Stumm, 1965; Collins and Buol, 1970). Conversely, when Fe oxides
386 are reduced by the flow of reducing groundwater, Fe^{2+} and Mn^{2+} are released. Moreover, Fe is
387 more likely to adsorb or form complexes with organic matter than is Mn (Hem, 1972). The
388 occurrence of Mn in the upgradient portions of the study area can be explained by its occurrence
389 coinciding with a larger range of Eh values than Fe, and because it is less reactive with organic
390 matter and thus does not form complexes with it.

391 *5.2 Origin and evolution of trace elements in rocks and their release into groundwater*

392 Ba is mostly found in host rock in the form of the barite mineral ($BaSO_4$). This mineral
393 formed chemically when Ba^{2+}, originating from rising hydrothermal fluids across the Grenville
394 shield (Carignan et al., 1997) to the surface, encountered sulfate-rich water, such as seawater. The
395 precipitation of barite mainly depends on the availability of sulfate (from seawater) and barium
396 (mainly from crystalline rocks), these two elements not being transported together. (Machel,
397 2001; Aquilina et al., 2011b, 1997). Barite is then trapped in carbonate rocks during diagenesis
398 (Paradis and Lavoie, 1996). The direct relationship between Ba and corrected ^{14}C ages (Fig. 7c)
399 also suggests that a long water-rock interaction time, as well as the quasi-absence of recharge

400 downgradient, is critical in the release of this element into groundwater, and leads to an increase
401 in Ba concentrations along the flow path.

402 Similarly, F^- has a hydrothermal origin and can precipitate under the form of fluorite
403 (CaF_2) in carbonate rocks during diagenesis, when it is in contact with calcium-rich water, such
404 as seawater. F^- can also be adsorbed in clays by exchange with OH^- under acidic conditions
405 (Savenko, 2001), as in the volcanic activity of the Paleozoic. Reactivation of the St. Lawrence rift
406 system occurred during the Devonian and Mesozoic (Carignan et al., 1997; Tremblay et al., 2013;
407 Bouvier et al., 2012) bringing additional hydrothermal fluids and leading to F and F-Ba veins
408 hosted in Cambro-Ordovician rocks (Carignan, 1989; Carignan et al., 1997). Dissolution of these
409 veins might be a secondary source of dissolved F and Ba in modern groundwater, but it is
410 unlikely to be the main source because of their low presence and distribution in the area (more to
411 be considered as recorders of past events).

412 The main process leading to Fe- and Mn- sulfide precipitation in rocks is the sulfide
413 biogenic or thermochemical reduction (Machel, 2001). Lorraine shales contain up to 1.5% Total
414 Organic Carbon (Lavoie et al., 2013). The availability of reactive sulfate and organic matter is the
415 main factor underlying the transport/concentration of either Fe or Mn sulfides (eqn. 3, 4) in
416 anoxic/high temperature conditions (eqn. 5), or oxides (Fe_2O_3 and MnO) in cooler/oxidant
417 conditions.

418 $$Fe^{2+} + H_2S \rightarrow FeS + 2H^+ \qquad (3)$$

419 $$FeS + H_2S \rightarrow FeS_2 + H_2 \qquad (4)$$

420 $2CH_2O + SO_4^{2-} \rightarrow 2HCO_3^- + H_2S$ (5)

421 The presence of pyrite (FeS_2) has been observed in Appalachian metasediments (Sassano and
422 Schrijver, 1989; and in the NSF-R7 drilled well of this study) and in the Utica and Lorraine
423 shales (Bérubé et al., 1986), confirming the formation of Fe sulfides in the region during the
424 Paleozoic. Mn nodules from the Ordovician were found in the Appalachians, close to the study
425 area, in the St. Daniel Fm. (Trottier et al., 1991). Major weathering episodes driven by massive
426 groundwater recharge during the Devonian last stage of Appalachian orogeny (Lavoie, 2008) led
427 to the oxidation of Fe and Mn sulfides (FeS_2 and MnS) present in rocks, the release of Fe^{2+} and
428 Mn^{2+} into the aqueous media, and precipitation in the form of Fe and Mn oxides (Fe_2O_3 and
429 MnO; Appelo and Postma, 2005). The later confinement provided by the Champlain Sea clay
430 deposits led to the progressive reduction of groundwater which triggered the reduction of Fe and
431 Mn oxides and sulfurs in the rock, and the release of Fe^{2+} and Mn^{2+} into groundwater.

432 The potential sources of Ba, F, Fe, and Mn are thus the Ordovician rocks of the St.
433 Lawrence Platform and the Appalachian Mountains. Enrichment of these elements could be
434 related to Paleozoic episodes of Mississippi Valley Type (MVT) ore deposition (Ingebritsen and
435 Sanford, 1998; Machel, 2001), as observed in the Beekmantown Group dolostones in New York
436 State and in Ontario (Benison and Lowenstein, 1997). Macro-evidence of MVT-related deposits
437 is a barite ore exploited near the town of Upton, 20 km west of the study area in the
438 Drummondville Olistostrome of mid-Ordovician age (Paradis and Lavoie, 1996). Migration of
439 Na-Ca-Cl and Na-Cl-Br brines (Bethke and Marshak, 1990; Sverjenski and Garven, 1992) is
440 believed to be the main mechanism of MVT ore concentration. Primary fluid inclusions in quartz,

441 calcite, and saddle dolomite of the Beekmantown dolostones indicate that the mineralizing fluids
442 were Na-Ca-Cl brines (Benison and Lowenstein, 1997, Aquilina et al., 2011a,b). Pinti et al.
443 (2011) studied the origin of Na-Ca-Cl brines (up to 350 g/L TDS) in the Beekmantown and
444 Chazy Groups at Becancour. They concluded that these brines could be of Devonian age, one of
445 the most prolific periods of MVT ore deposition in North America (Garven et al., 1993).

446 *5.3 Groundwater residence times and their relationship with excess trace ion concentrations*

447 Corrected ^{14}C ages range from 17,050±3410 yrs for NSF-R1 to 283±57 yrs for NSF219
448 (Table 1). The older ^{14}C age corresponds to a period when the Laurentide Ice Sheet covered the
449 study area. However, as a result of the geothermal gradient, as well as the heat generated by
450 friction, meltwater was present at the base of the continental glaciers (e.g., Gilkeson et al., 1981).
451 There is compelling evidence that the magnitude of subglacial recharge into confined aquifer
452 systems covered by the Laurentide Ice Sheet was up to 10 times greater than at present (e.g.,
453 McIntosh and Walter, 2005; Person et al., 2007). The other corrected ^{14}C ages obtained in the
454 NSF watershed range between 12,000 and modern (Table 1), similar to the ^{14}C ages found in the
455 neighboring watersheds of Becancour (corrected ^{14}C from 9,200 to modern; Vautour et al., 2015)
456 and Eastern Monteregie (uncorrected ^{14}C ages from 13,800 to modern; Beaudry, 2013). This
457 period roughly corresponds to the ice retreat of the Laurentide Ice Sheet, followed by a glacio-
458 isostatic marine transgression, known as the Champlain Sea, which invaded the study area
459 12,800-12,300 yrs ago (Parent et al., 1985). Between 10,600 and 6,700 yrs before present, the
460 main phase of isostatic rebound lowered the St. Lawrence River base level from +60 m asl to ca.
461 16 m asl (Lamarche et al., 2007). At 6.7 kyrs, the hydrographic network of the St. Lawrence

462 Valley reached a configuration close to that observed at present. It is expected that during this
463 accelerated isostatic rebound period, new emerging recharge zones and increased potentiometric
464 heads favored a large invasion of meltwater into the shallower Quaternary aquifers (e.g., Person
465 et al., 2007) and the confined aquifers of the St. Lawrence Lowlands.

466 In the Michigan basin, large amounts of meltwater resulted in the dissolution of Devonian
467 evaporites, which increased the groundwater salinity (e.g., McIntosh et al., 2011). In a broad
468 region of the Cambrian-Ordovician aquifer system of northeastern Illinois, dissolution of
469 secondary barite, driven by meltwater infiltration, led to high dissolved barium concentrations in
470 groundwater (Gilkeson et al., 1981). In the St. Lawrence Lowlands, a similar process could have
471 taken place. During subglacial recharge under the Laurentide Ice Sheet at around 20,000 yrs
472 (Person et al., 2007), a large amount of meltwater could have favored the dissolution of
473 secondary barite, which was subsequently diluted by the last episode of meltwater formation
474 during the Laurentide Ice Sheet retreat (12,000 yrs), and the reorganization of the hydrographic
475 network of the St. Lawrence Lowlands (6700 yrs and younger) (Fig. 7c).

476 Similar results have been recently showed in the Armorican basement in terms of ages and
477 links between elements dissolved in old groundwater and glacial transport which supports the
478 groundwater evolution model presented in this study (Aquilina et al., 2015).

479

480 **6. CONCLUSIONS**

481 The objective of this study was to establish links between groundwater quality,
482 groundwater residence times, and regional geology on the scale of the St. Lawrence Platform and
483 the Appalachian Mountains aquifers in southern Quebec (Canada). To attain this objective, the
484 study combined groundwater chemistry and groundwater residence times with an economic
485 geology model and historical geology.

486 Results have shown that major ion concentrations highlight regional groundwater flow
487 directions and the evolution of groundwater from a young water end-member, characterized by
488 the Ca-HCO_3 water type in the piedmont of the Appalachians recharge area, to an old water end-
489 member, characterized by the Na-HCO_3 type downgradient in the study area. Two distinct water
490 masses were identified, with $^{3}H/^{3}He$ ages pointing to water less than 60 years, and ^{14}C ages of
491 several thousand years, likely infiltrated in the Cambro-Ordovician aquifers by subglacial
492 recharge or immediately following the last deglaciation. This long interaction time between rock
493 and groundwater is likely an important factor in the release of anomalous concentrations of Ba, F,
494 Fe, and Mn into groundwater. Their concentrations in the rock can be explained by their
495 deposition as mineral phases (barite, sulfates, etc.) in the sedimentary rocks of the Cambro-
496 Ordovician St. Lawrence Platform and Appalachians. Their recent release in post-glacial
497 groundwater might be favored by the redox state, geology, pH, interaction with organic matter,
498 and availability of reactive dissolved compounds, such as SO_4^{2-}. This work shows that the release
499 of hydrothermal fluids along regional faults in the sedimentary basin, combined with marine
500 water, has likely triggered the deposition of sulfides in reducing environments and the deposition
501 of oxides in oxidizing environments.

This study brings a new and original understanding of the groundwater system within the context of its geological history. It not only characterizes the natural groundwater quality of the study area, but also contributes to better understanding groundwater quality problems in the St. Lawrence Lowlands. A similar approach to understanding natural groundwater quality problems could be used in similar geological settings, such as in the Paleozoic sedimentary basins of Michigan or Mississippi, for example, but may also be applied in different geological contexts, such as volcanic or plutonic settings.

ACKNOWLEDGMENTS

The authors would like to thank the Quebec Ministry of Environment (Ministère du Développement durable, de l'Environnement et de la Lutte contre les changements climatiques), the Quebec Research Fund ("Fonds de recherche du Québec - Nature et Technologies"), as well as the "Municipalités régionales de comtés-MRC", the "Conseil régional des élus-CRE", the municipalities, and the well owners who contributed funding to this research and access to sampling locations. We wish to thank Chris Hall of the University of Michigan (USA) for analyzing helium isotopes, and Pauline Méjean for helping with the analyses during her stay at AORI, University of Tokyo (Japan). Michelle Laithier (UQAM) is thanked for having redrawn the figures of this manuscript.

REFERENCES

Aeschbach-Hertig, W., Gleeson, T., 2012. Regional strategies for the accelerating global problem of groundwater depletion. Nat. Geosci. 5, 853-861.

Andrews, J.N., 1985. The isotopic composition of radiogenic helium and its use to study groundwater movement in confined aquifers. Chem. Geol. 49, 339-351.Appelo C.A.J., Postma, D. (2005). Geochemistry, groundwater and pollution, 2nd edn. CRC Press, Boca Raton, Florida, USA.

Aquilina L., Vergnaud-Ayraud V. Armandine Les Landes A. Pauwels H. Davy P. Pételet-Giraud E., T., Roques C., Chatton E., Bour O., Ben Maamar S., Dufresne A., Khaska M., Le Gal La Salle C., Barbecot F. 2015. Impact of climate changes during the last 5 million years on groundwater in basement aquifers. Scientific Reports 5, 14132.

Aquilina, L., De Dreuzy, J.R., 2011a. Relationship of present saline fluid with paleomigration of basinal brines at the basement/sediment interface (Southeast basin – France). Appl. Geochem. 26, 1933-1945.

Aquilina L., Boulvais P., Mossmann J.R., 2011b. Fluid migration at the basement/sediment interface along the marginof the South-East Basin (France) : implications for Pb-Zn ore formation. Miner. Deposita 46-8, 959-979.

Aquilina L., Pauwels H. and Fouillac C., 1997. Water-rock interaction processes in the Triassic sandstone and the granitic basement of the Rhine graben : geochemical investigation of a geothermal reservoir, Geochim. et Cosmochim. Acta 61-20, p. 4281-4295.

Barbecot, F., Marlin, C., Gibert, E., Dever. L., 2000. Hydrochemical and isotopic characterisation of the Bathonian and Bajocian coastal aquifer of the Caen area (northern France). Appl. Geochem. 15, 791-805.

Beaudry, C., 2013. Hydrogéochimie de l'aquifère rocheux régional en Montérégie est, Québec. MS Thesis. Institut national de la recherche scientifique (INRS), Quebec, Canada.

Benison, K.C., Lowenstein, T.K., 1997. Carbonate-hosted mineralization of the Lower Ordovician Ogdensburg Formation: Evidence for a Paleozoic thermal anomaly in the St. Lawrence lowlands of New York and Ontario. In: Montenez, I., Shelton, K., Gregg, J., (Eds.), Basin-wide fluid flow and associated diagenetic patterns: Integrated petrologic, geochemical, and hydrologic considerations. SEPM Spec. Publ. 57, 207-218.

Benson, B.B., Krause, D., 1980. Isotopic fractionation of helium during solution: A probe for the liquid state. J. Sol. Chem. 9, 895-909.

Bérubé, M.-A., Locat, J., Gélinas, P., Chagnon, J.-Y., Lefrançois, P., 1986. Black shale heaving at Sainte-Foy, Quebec, Canada. Can. J. Earth Sci. 23, 1774-1781.

Bethke, C.M., Marshak, S., 1990. Brine migrations across North America — The plate tectonics of groundwater. Annu. Rev. Earth Planet. Sci. 18, 287-315.

Bolduc, A.M., Ross, M., 2001. Surficial geology, Lachute-Oka, Québec. Geol. Surv. Can. Open File 3520.

559 Bouvier, L., Pinti, D.L., Tremblay, A., Minarik, W., Roden-Tice, M., 2012. Late Jurassic
560 reactivation of the St. Lawrence rift system, Québec, Canada: evidence from apatite (U-Th)/He
561 dating. Proc. 3rd INQUA-IGCP-567 Inter. Workshop Active Tectonics, Paleoseismology &
562 Archaeoseismology, 25-28.

563 Carignan, J., 1989. Caractérisations isotopiques (C, O, Sr, Pb) et genèse de filons épithermaux
564 associés au rift du Saint-Laurent. MS thesis, Université du Québec à Montréal, Quebec, Canada.

565 Carignan, J., Gariépy, C., Hillaire-Marcel, C., 1997. Hydrothermal fluids during Mesozoic
566 reactivation of the St. Lawrence rift system: C, O, Sr and Pb isotopic characterization. Chem.
567 Geol. 137, 1-21.

568 Carrillo-Rivera, J.J., Cardona, A., Edmunds, W.M., 2002. Use of abstraction regime and
569 knowledge of hydrogeological conditions to control high-fluoride concentration in abstracted
570 groundwater: San Luis Potosì basin, Mexico. J. Hydrol. 261, 24–47.

571 Castro, M.C., Goblet, P., 2005. Calculation of Groundwater ages – a Comparative Analysis.
572 Ground Water 43, 368-380.

573 Castro M.C., Ma L., Hall, C.M., 2009. A primordial, solar He-Ne signature in rcrustal fluids of a
574 stable continental region. Earth Planet. Sci. Lett. 279, 174-184.

575 Clark, I.D., Fritz, P., 1997. Environmental Isotopes in Hydrogeology. CRC Press, Boca Raton,
576 Florida, USA.

577 Cloutier, V., Lefebvre, R., Savard, M.M., Bourque, É., Therrien, R., 2006. Hydrogeochemistry
578 and groundwater origin of the Basses-Laurentides sedimentary rock aquifer system, St. Lawrence
579 Lowlands, Quebec, Canada. Hydrogeol. J. 14, 573-590.

580 Cloutier, V., Lefebvre, R., Savard, M.M., Therrien, R., 2010. Desalination of a sedimentary rock
581 aquifer system invaded by Pleistocene Champlain Sea water and processes controlling
582 groundwater geochemistry. Environ. Earth Sci. 59, 977-994.

583 Collins, J.F., Buol, SW., 1970. Effects of fluctuations in the Eh–pH environment on iron and/or
584 manganese equilibria. Soil Sci. 110, 111-118.

585 Eichinger, L., 1983. A contribution to the interpretation of ^{14}C groundwater ages considering the
586 example of a partially confined sandstone aquifer: Radiocarbon 25, 347–356.

587 Environment Canada. 2014. Canadian climate normals 1961-2010
588 (http://climat.meteo.gc.ca/climate_normals/results_1981_2010_f.html?stnID=5426&autofwd=1).

589 Evans, G.V., Otlet, R.L., Downing, A., Monkhouse, R.A., Rae, G., 1979. Some problems in the
590 interpretation of isotope measurements in United Kingdom aquifers. In: Isotope Hydrology II.
591 International Atomic Energy Agency, Vienna, 679-708.

592 Fontes C.H., 1992. Chemical and isotopic constraints on ^{14}C dating of groundwater. In: Taylor,
593 R.E., Long, A., Kra R.S. (Eds.), Radiocarbon dating After Four Decades: An Interdisciplinary
594 Perspective, Springer, New York, 242–26.

595 Garven, G., Ge, S., Person, M.A., Sverjensky, D.A., 1993, Genesis of stratabound ore deposits in
596 the midcontinent basins of North America. 1. The role of regional groundwater flow. Am. J. Sci.
597 293, 497-568.

598 Gilkeson, R.H., Perry, E. Jr., Cartwright, K., 1981. Isotopic and geologic studies to identify the
599 sources of sulfate in groundwater containing high barium concentrations. University of Illinois
600 Water Resour. Center Report 81-0165, 39 p.

601 Globensky, Y., 1987. Géologie des Basses-Terres du Saint-Laurent, Quebec. Ministère des
602 Richesses Naturelles du Quebec 63 (v. MM 85-02).

603 Globensky, Y., 1993. Lexique stratigraphique canadien. Volume V-B: région des Appalaches,
604 des Basses-Terres du Saint-Laurent et des Iles de la Madeleine. Ministère de l'Énergie et des
605 Ressources et Direction Générale de l'Exploration géologique et minérale, DV 91e23.

606 GRIES, 2011. Protocole de prélèvement d'échantillons d'eau souterraine pour le PACES. Juin
607 2010, 9 p.

608 Health Canada, 2014. Guidelines for Canadian drinking water quality: summary table. Federal–
609 Provincial–Territorial Committee on Drinking Water. http://www.hc-sc.gc.ca/ewh-semt/water-
610 eau/drink-potab/guide/index-eng.php

611 Heemskerk, A.R., Johnson, J., 1998. Tritium analysis: technical procedure 1.0. University of
612 Waterloo, Waterloo, Ontario, Canada.

613 Hem, J.D., 1972. Chemical factors that influence the availability of iron and manganese in
614 aqueous systems. Geol. Soc. Am. Bull. 83, 443-50.

615 Homoncik, S.C., MacDonald, A.M., Heal, K.V., Dochartaigh, B.E.O., Ngwenya, B.T., 2010.
616 Manganese concentrations in Scottish groundwater. Sci. Total Environ. 408, 2467-2473.

617 Hounslow, AW., 1995. Water quality data: Analysis and interpretation. CRC Press, Boca Raton,
618 Florida, USA.

619 Ingebritsen, S.E., Sanford, W.E., 1998 Groundwater in geologic processes. Cambridge University
620 Press. Cambridge, United Kingdom.

621 Kloppmann, W., Girard, J.P., Négrel, P., 2002. Exotic stable isotope compositions of saline
622 waters and brines from crystalline basement. Chem. Geol. 184, 49–70.

623 Lacasse, K., 2013. Caractérisation géochimique et isotopique des aquifères du sud-ouest de la
624 Mauricie. MS thesis, Université du Québec à Trois-Rivières, Quebec, Canada.

625 Lamarche, L., Bondue, V., Lemelin, J.-M., Lamothe, M., Roy, M., 2007. Deciphering the
626 Holocene evolution of the St. Lawrence River drainage system using luminescence and
627 radiocarbon dating. Quarter. Geochr. 2, 155-161. doi:10.1016/j.quageo.2006.04.002

628 Lamothe, M., St-Jacques G., 2014. Géologie du Quaternaire des bassins versant des rivières
629 Nicolet et Saint-François, Québec. Ministère Energies et Ressources Naturelles Report, 34 p.

630 Lamothe, M., 1989. A new framework for the Pleistocene stratigraphy of the central St.
631 Lawrence Lowland, southern Quebec. Géogr. Phys. Quarter. 43, 119–129.

Larocque, M., Gagné S., Tremblay L., Meyzonnat G., 2015. Rapport d'étape Phase III. Projet de connaissance des eaux souterraines de la zone Nicolet et de la partie basse de la zone Saint-François. Report presented to the MDDELCC, 261 p.

Lavoie, D., 2008. Appalachian Foreland Basin in Canada, In: Hsü, K.J., Miall, A.D. (Eds.), Sedimentary Basins of the World, series ed. Sedimentary Basins of the World — USA and Canada, vol. 5. Elsevier, Amsterdam, pp. 65-103.

Lavoie, D., Rivard, C., Lefebvre, R., Sejourne, S., Theriault, R., Duchesne, M.J., Ahad, J.M.E., Wang, B., Benoit, N., Lamontagne, C., 2013. The Utica Shale and gas play in southern Quebec: geological and hydrogeological syntheses and methodological approaches to groundwater risk evaluation. Inter. J. Coal Geol. 126, 77-91.

LECO Corporation, 2007. Carbon and Sulfur Determination – LECO Induction Furnace Instruments. 48 pp.

Li, J., Wang, Y., Xie, X., Su, C., 2012. Hierarchical cluster analysis of arsenic and fluoride enrichments in groundwater from the Datong basin, Northern China. J. Geochem. Explor. doi:10.1016/j.gexplo.2012. 05.002.

Ma, L., Castro, M.C., Hall, C.M., Lohmann, W.M., 2005. Cross-formational flow and salinity sources inferred from a combined study of helium concentrations, isotopic ratios and major elements in the Marshall aquifer, southern Michigan. Geochem. Geophys. Geosyst., 6, Q10004, doi:10.1029/2005GC001010.

651 Maclear, L. G. A., Adlem, M., Libala, M. B., 2003. Trend analysis of fluoride concentrations in
652 surface water and groundwater: 2000–2003. Coelga Devel. Co, Report 258047/6.

653 Machel, H.G., 2001. Bacterial and thermochemical sulfate reduction in diagenetic settings—old
654 and new insights. Sediment. Geol. 140, 143-175.

655 Mahlknecht, J., Steinich, B., Leon, I. N., 2004. Groundwater chemistry and mass transfers in the
656 independence aquifer, central Mexico, by using multivariate statistics and mass balance models.
657 Environ. Geol. 45, 781–795.

658 Marimon, M.P.C., Roisenberg, A., Suhogusoff A.V., Viero A.P., 2012. Hydrogeochemistry and
659 statistical analysis applied to understand fluoride provenance in the Guarani Aquifer System,
660 Southern Brazil. Environ. Geochem. Health. 35, 391-403.

661 Matsuda, J., Matsumoto, T., Sumino, H., Nagao, K., Yamamoto, J., Miura, Y., Kaneoka, I.,
662 Takahata, N., Sano, Y., 2002. The $^{3}He/^{4}He$ ratio of the new internal He Standard of Japan
663 (HESJ). Geochem. J. 36, 191-195.

664 McIntosh, J.C., Walter, L.M., 2005. Volumetrically significant recharge of Pleistocene glacial
665 meltwaters into epicratonic basins: Constraints imposed by solute mass balances. Chem. Geol.
666 222, 292-309.

667 McIntosh, J.C., Garven, G., Hanor, J.S., 2011. Impacts of Pleistocene glaciation on large-scale
668 groundwater flow and salinity in the Michigan Basin. Geofluids 11, 18-33.

669 MDDELCC, 2012. Stratégie de protection et de conservation des sources destinées à
670 l'alimentation en eau potable. Available at
671 http://www.mddelcc.gouv.qc.ca/eau/potable/strategie/strategie.pdf

672 Méjean, P., Pinti, D.L., Larocque, M., Sano, Y., 2015. Noble gas, carbon and nitrogen in a St.
673 Lawrence Lowlands bedrock aquifer (eastern Canada). Abstract 34178 presented at AGU Joint
674 Assembly, Montréal, QC, 3-7 May.

675 Meyzonnat, G., Larocque M., Barbecot, F., Gagné, S., Pinti, D.L., 2015. The potential of major
676 ion chemistry to assess groundwater vulnerability of a regional aquifer in southern Quebec
677 (Canada). Environm. Earth Sci., in press.

678 Mook, WG., 1972. On the reconstruction of the initial ^{14}C content of groundwater from the
679 chemical and isotopic composition. In: Rafter, T.A., Grant Taylor, T. (Eds.), Proceedings of the
680 8th International ^{14}C Conference. Wellington, Royal Society of New Zealand: 342-352.

681 Morgan, J.J., Stumm, W., 1965. The role of multivalent metal oxides in limnological
682 transformations, as exemplified by iron and manganese. In: Jaag O. (Ed.). Proc. Second Intern.
683 Conf. August 1964, Tokyo. Advances in Water Pollution Research, Pergamon Press. pp. 103-31.

684 Nickson, R.T., McArthur, J.M., Burgess, W.G., Ahmed, K.M., Ravenscroft, P. and Rahman, M.,
685 1998. Arsenic poisoning of Bangladesh groundwater. Nature 395, 338.

686 Ozima, M., Podosek, F.A., 1983. Noble Gas Geochemistry. Cambridge University Press,
687 Cambridge, United Kingdom.

688 Pacheco, F.A.L., 1998. Application of correspondence analysis in the assessment of groundwater
689 chemistry. Math. Geol. 30, 129–161.

690 Paradis, S., Lavoie, D., 1996, Multiple-stage diagenetic alteration and fluid history of Ordovician
691 carbonate-hosted barite mineralization, southern Quebec Appalachians: Sediment. Geol. 107,
692 121–139.

693 Paralta, E., Ribeiro, L., 2001. Stochastic modeling and probabilistic risk maps of nitrate pollution
694 in the vicinities of Beja (Alentejo, South Portugal). Proc. 3rd International Conference on Future
695 Groundwater Resources at Risk, Lisbon, 251-261.

696 Parent, M., Dubois, J.M.M., Bail, P., Larocque, A., Larocque, G., 1985. Paléogéographie du
697 Quebec méridional entre 12 500 et 8000 ans BP. Recherches Amérindiennes au Quebec 15, 17–
698 37.

699 Patriarche, D., Castro M.C., Goblet P., 2004. Large-scale hydraulic conductivities inferred from
700 three dimensional groundwater flow and 4He transport modeling in the Carrizo aquifer. Texas, J.
701 Geophys. Res., 109, B11202, doi:10.1029/2004JB003173.

702 Pearson, F.J., 1992. Effects of parameter uncertainty in modeling ^{14}C in groundwater. In: In:
703 Taylor, R.E., Long, A., Kra R.S. (Eds.), Radiocarbon dating After Four Decades: An
704 Interdisciplinary Perspective, Springer, New York, 262–275.

705 Person, M., McIntosh, J., Bense, V., Remenda, V.H., 2007. Pleistocene hydrology of North
706 America: The role of ice sheets in reorganizing groundwater flow systems. Rev. Geophys. 45, 1-
707 28.

708 Pinti, D.L., Béland-Otis, C., Tremblay, A., Castro, M.C., Hall, C.M., Marcil, J.-S., Lavoie, J.-Y.,
709 Lapointe, R., 2011. Fossil brines preserved in the St-Lawrence Lowlands, Quebec, Canada as
710 revealed by their chemistry and noble gas isotopes, Geochim. Cosmochim. Acta 75, 4228-4243.

711 Plummer, L.N., Glynn, P.D., 2013. Radiocarbon dating in groundwater systems. In: Isotope
712 methods for dating old groundwater. International Atomic Energy Agency, Vienna, 33-89.

713 Salem, O., Visser, J.H., Dray, M., Gonfiantini, R., 1980. Groundwater flow patterns in the
714 western Lybian Arab Jamahiriaya. In: Arid-Zone Hydrology: Investigations with Isotope
715 Techniques. International Atomic Energy Agency, Vienna, 165-179.

716 Sano, Y., Fischer T., 2013. The analysis and interpretation of noble gases in
717 modern hydrothermal systems. In: Burnard, P. (Ed.), The Noble Gases as Geochemical Tracers,
718 Advances in Isotope Geochemistry series, Springer, New York, 249-317.

719 Sano, Y., Tokutake, T., Takahata, N., 2008. Accurate measurement of atmospheric helium
720 isotopes. Anal. Sci. 24, 521-525.

721 Sassano, G.P., Schrijver, K, 1989. Framboidal pyrite early-diagenetic, late-
722 diagenetic and hydrothermal Occurrences from the Acton Vale Quarry, Cambro-Ordovician,
723 Qc., Am. J. Sci. 289, 167-179.

724 Savenko, A.V., 2001. Interaction between clay minerals and fluoride-containing solutions. Water
725 Resour. Res. 28, 274–277.

726 Schlosser, P., Stute, M., Sonntag, C., Munnich, K.O., 1989. Tritiogenic ^{3}He in shallow
727 groundwaters. Earth Planet. Sci. Lett. 94, 245-256.

728 SIGEOM, 2014. Carte intéractive. Ministère des Ressources Naturelles du Québec. Available at :
729 http://sigeom.mrn.gouv.qc.ca/signet/classes/I1108_afchCarteIntr?l=f

730 Smith, S.P., Kennedy, B.M., 1983. The solubility of noble gases in water and NaCl brine.
731 Geochim. Cosmochim. Acta. 47, 503-515.

732 Sverjenski, D.A., Garven, G., 1992. Tracing great fluid migrations. Nature 356, 481-482.

733 Tamers, M.A., 1967. Radiocarbon ages of groundwater in an arid zone unconfined aquifer. In
734 Isotope Techniques in the Hydrological Cycle. AGU Geophys. Monogr. 11, 143-152.

735 Tremblay, A., Roden-Tice, M.K., Brandt, J.A., Megan, T.W., 2013. Mesozoic fault reactivation
736 along the St. Lawrence rift system, Eastern Canada: thermochronologic evidence from apatite
737 fission-track dating. Geol. Soc. Am. Bull. 125, 794-810.

738 Trottier, J., Brown, A.C., Gauthier, M., 1991. An Ordovician rift environment for the
739 Memphremagog polymetallic massive sulphide deposit, Appalachian Ophiolite Belt, Quebec.
740 Can. J. Earth Sci. 28, 1887-1904.

741 Vautour, G, Pinti, D.L., Méjean, P., Saby, M., Meyzonnat, G., Larocque, M., Castro, M.C., Hall,
742 C.M., Boucher, C., Roulleau, E., Barbecot, F., Takahata, N., Sano, Y., 2015. $^{3}H/^{3}He$, ^{14}C and (U-
743 Th)/He groundwater ages in the St. Lawrence Lowlands, Quebec, Eastern Canada. Chem. Geol.
744 413, 94-106, 10.1016/j.chemgeo.2015.08.003.

745 Weise, S., Moser, H., 1987. Groundwater dating with helium isotopes. In: Techniques in Water
746 Resource Development. International Atomic Energy Agency, Vienna , 105-126.

747 Weiss, R.F., 1968. Piggybacks sampler for dissolved gas studies on sealed water tubes. Deep Sea
748 Res. 15, 695-699.

749

FIGURE CAPTIONS

Figure 1 a) Geological map of the St. Lawrence Lowlands (southern Quebec, Canada) and location of the Nicolet-Saint-François study area and b) geological profile along the regional flow line.

Figure 2 Sampling sites for geochemical, ^{3}H, ^{14}C, $\delta^{13}C$, and noble gas analyses overlain on the spatial distribution of confinement conditions (modified from Larocque et al., 2013).

Figure 3 Piper diagram of groundwater hydrogeochemistry representing groundwater types of the study area.

Figure 4 Evidence of groundwater geochemistry evolution; a) cationic exchange between Ca^{2+} and Na^{+} in groundwater and evidence of salt water (the arrow represents the general groundwater flow path), and b) evolution of the Mg/Ca ratio plotted against pH, indicating the dissolution of carbonates along the flow line.

Figure 5 Measured $^{3}He/^{4}He$ ratios corrected for helium air excess (He_{ea}) (and normalized to the $^{3}He/^{4}He$ atmospheric ratio) versus the relative amount of ^{4}He due to solubility ($^{4}He_{eq}$) with respect to total helium corrected for air excess. The dashed line represents the mixing line between recharge water (air saturated water conditions, or ASW, with $^{3}He/^{4}He$ ratio = R_{eq}) and water enriched in terrigenic ^{4}He (R_{Terr}). Dashed and dotted lines represent the addition of helium, and mixing with a terrigenic component of ratio R_{terr}.

Figure 6 a) Inverse trends between the measured ^{14}C activity ($A^{14}C$) and the measured $\delta^{13}C$ of the TDC (b). Dead carbon reservoir isotopic composition and ^{14}C activities are from Taupin (1990) (soil CO_2) and Le Gal Lasalle et al. (2001) (carbonates) and b) measured ^{3}H activity against the uncorrected ^{14}C activity ($A^{14}C$). Numbers on the theoretical mixing line represent the percentage of the older component in the mixture.

Figure 7 a) ^{14}C ages as a function of the corresponding Mg/Ca ratio, b) evolution of the ^{3}H activity as a function of the Mg/Ca ratio, and c) relationship between ^{14}C ages and barium (Ba) concentrations.

Figure 8 Relationship between barium (Ba) concentrations and the distance along the flow line, with geology superposed in the background.

Figure 9 a) Relationship between F and Ca (the dashed line represents the dissolution curve of calcium fluorine), and b) evolution of F as a function of pH.

Figure 10 Relationships between a) pH and Eh, compared to the Fe/Mn ratio represented by the size of the circles, and b) Mn concentrations and Fe concentrations, illustrated for the different water types.

Table 1. *^{3}H-^{3}He and ^{14}C ages of groundwater from the Nicolet Saint-François study area.*

Well name	^{3}H	±	$^{3}He_{tri}$	±	^{3}H-^{3}He	±	$A^{14}C$	±	$\delta^{13}C$	^{14}C	^{14}C
	TU		ccSTP/g x 10^{-13}		age yrs		pMC		‰ V-PDB	ages (yrs) ±0.5% Uncorrected	ages (yrs) ±20% Corrected
NSF134	8.8	1.0	1.10	0.10	30.90	1.66	60.8	0.2	-10.7	4113	2140
NSF137	5.2	0.8	7.92	0.61	>60						
NSF140	9.8	1.0	0.23	0.11	12.17	0.90					
NSF144	1.4	0.6	1.57	0.06	56.10	7.29	56.1	0.20	-16.3	4778	6280
NSF148	8.3	0.7	2.63	0.08	46.80	1.39					
NSF149	4.5	0.5	5.19	0.50	>60						
NSF150	10.9	0.9	13.50	1.32	>60						
NSF152	4.8	0.6	1.82	0.13	50.24	2.09					
NSF215	10.5	1.1	0.08	0.05	4.78	0.44	94.7	0.4	-20	450	1310
NSF216	9.8	0.8	5.93	1.29	58.28	1.40	90.6	0.3	-22.1	816	4860
NSF218*	11.9	1.0	5.83	0.72	54.06	1.42	85.2	0.3	-18.6	1324	2880
NSF219*	12.7	1.0	6.51	3.36	55.70	1.34	97.3	0.4	-20.3	226	280
NSF220	5.1	0.6	1.78	0.10	48.25	1.95	43.5	0.2	-16	6881	8200
NSF221	5	0.6	6.39	1.95	>60		24.3	0.2	-12.3	11695	10210
NSF224	0.8	0.3	1.39	0.18	>60						
NSF242	10.2	1.0	0.14	0.06	7.94	0.63					
NSF244	10	1.0	0.47	0.06	19.28	1.18					
NSFR1	0.8	0.6	-0.58	1.38	>60		6.5	0.1	1.9	22596	17050
NSFR4	3.2	0.6	2.12	0.12	60.02	3.22					
NSFR7	9.8	1.0	0.67	0.10	23.55	1.33	65.4	0.2	-17.7	3510	3690

All ^{14}C ages corrected using the Fontes and Garnier equilibrium model (Fontes. 1992), except for NSFR1 (Tamers. 1975).

* granular wells

Table 2. *Chemical analyses of rocks from the Nicolet Saint-François study area*

Well name	CaO	MgO	Na_2O	K_2O	TOT/S	TOT/C	Ba	F	Fe_2O_3	MnO
	%	%	%	%	%	%	ppm	ppm	%	%
NSF-R1	6.62	3.25	1.05	3.3	0.13	1.68	345	896	6.1	0.12
NSF-R2	35.81	1.45	0.4	1	0.35	8.53	244	650	1.7	0.03
NSF-R3	2.76	2.64	1.74	1.04	0.79	1.17	1055	905	4.87	0.16
NSF-R7	1.05	1.7	1.21	3.2	<0.02	0.15	692	717	8.55	0.11
NSF-R8	3.33	3.64	0.99	3.16	0.35	0.82	485	794	5.81	0.18
NSF-R9	39.22	3.14	0.38	0.36	0.1	10.09	124	386	1.27	0.03
NSF-R10	10.69	3.1	0.97	3.68	0.81	3.16	223	955	4.91	0.07

Table 3: Chemical interpretation for each cluster from the results of a hierarchical cluster analysis

Clusters	C1	C2	C3	C4	C5	C6	C7
Number of samples	34	18	9	13	26	45	7
Ca	67,82	84,72	**114,44**	13,89	30,56	36,91	0,33
Mg	12,80	15,76	**24,21**	5,52	11,32	6,25	0,06
Na	17,14	147,50	24,22	146,23	22,84	8,15	**185,71**
K	2,19	4,12	**6,48**	2,17	4,23	1,71	2,38
HCO_3	188,24	252,39	**343,33**	256,15	159,42	98,07	275,71
Cl	22,07	**214,63**	22,81	72,37	3,93	11,72	43,00
SO_4	32,00	**60,28**	48,11	8,54	7,00	12,22	48,57
F	0,11	0,44	0,12	**1,00**	0,24	0,04	0,11
Mn	0,26	0,41	**0,64**	0,03	0,13	0,02	0,00
Fe	0,10	0,17	**2,64**	0,16	0,28	0,00	0,00
Ba	0,09	0,60	**0,72**	0,47	0,29	0,02	0,00
Groups	Ca-HCO3	Na-HCO3	Ca-HCO3	Na-HCO3	Mix-HCO3	Ca-HCO3	Na-HCO3
Dominant trace elements	Mn	Ba, F,	Fe, Mn, Ba	F			

Bold values: highest values of all clusters for the given element; underlined values: lowest values of all clusters for the given element

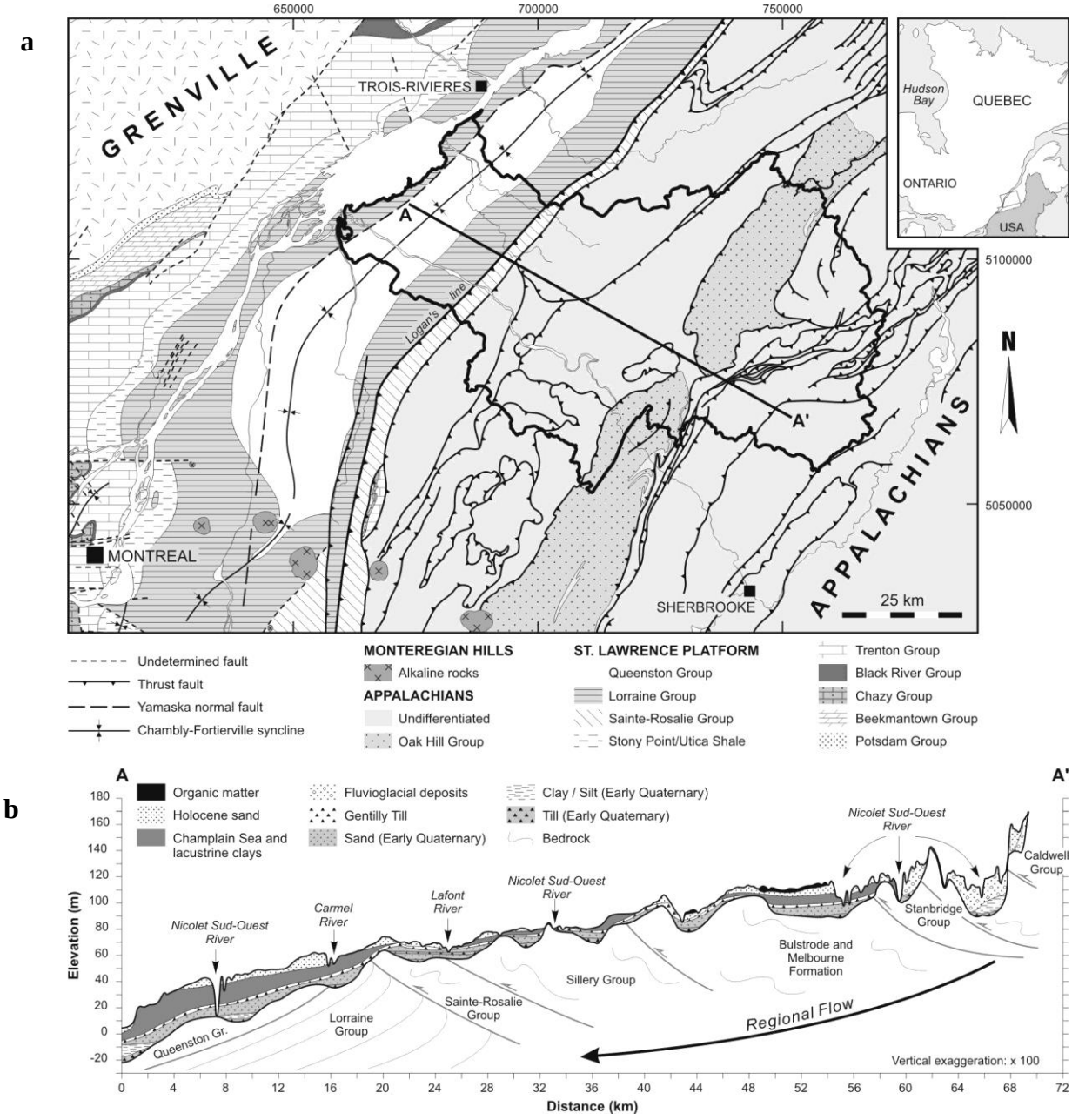

Saby et al. (2015)

Figure 1

Applied Geochemistry – To be submitted

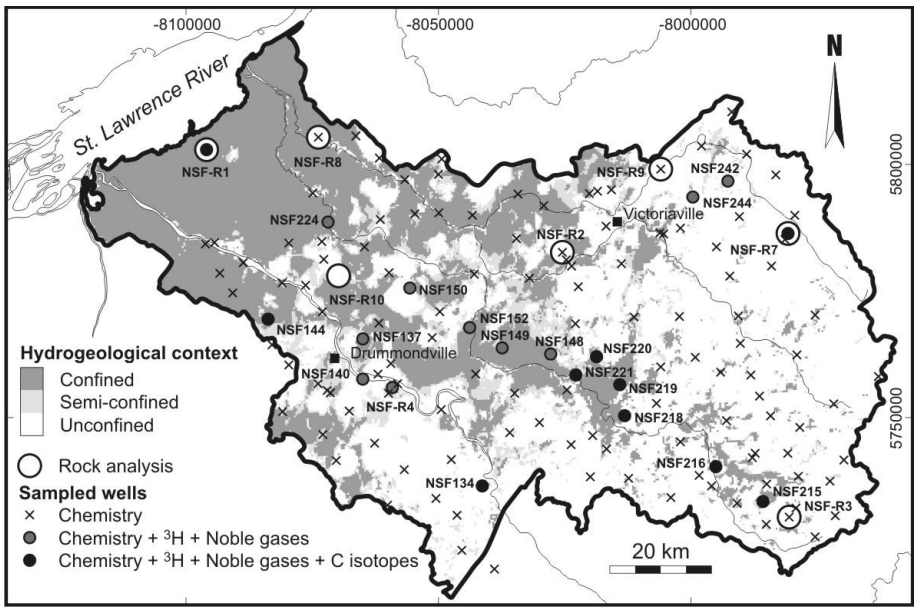

Saby et al. (2015)

Figure 2

Applied Geochemistry – To be submitted

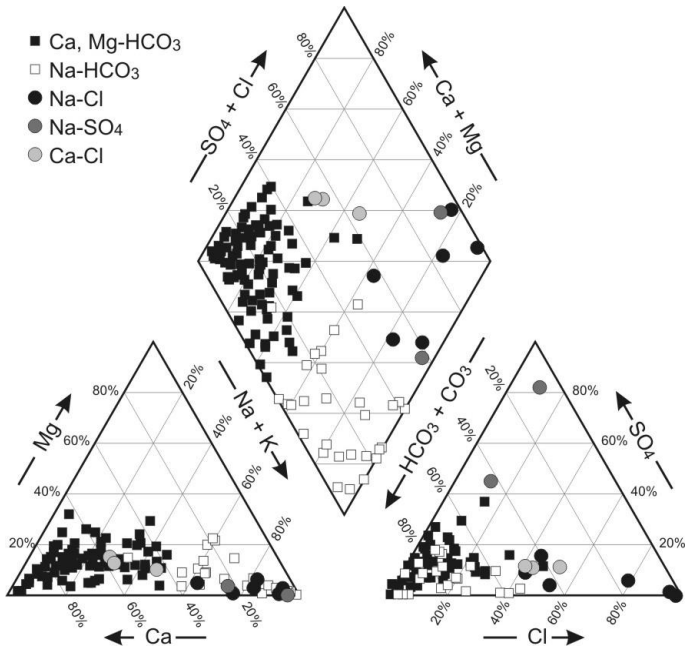

Saby et al. (2014)

Figure 3

Applied Geochemistry – To be submitted

a

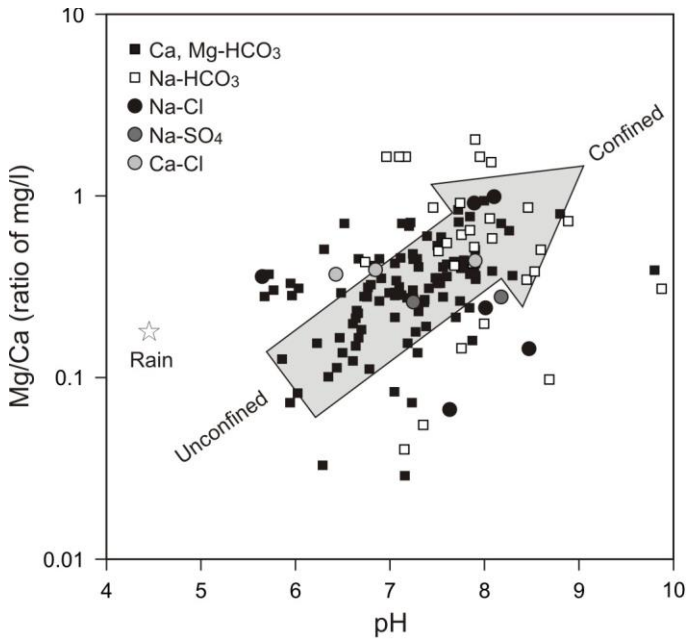

b

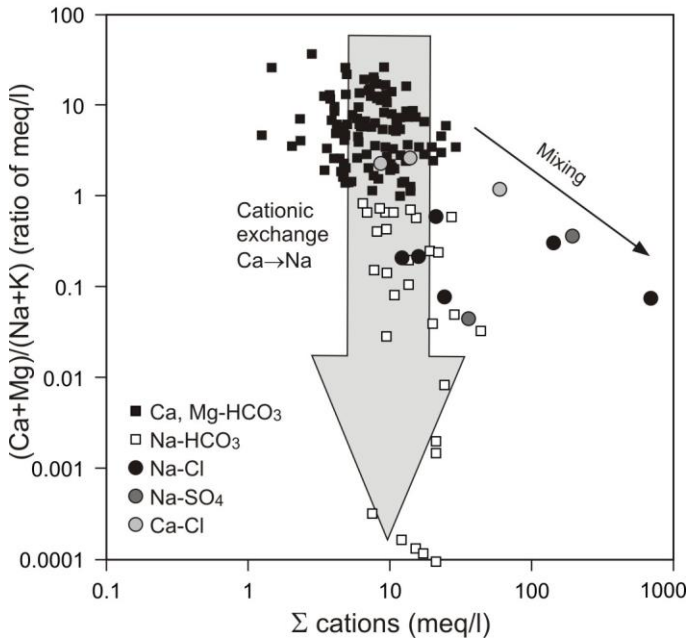

Saby et al. (2015)

Figure 4

Applied Geochemistry – To be submitted

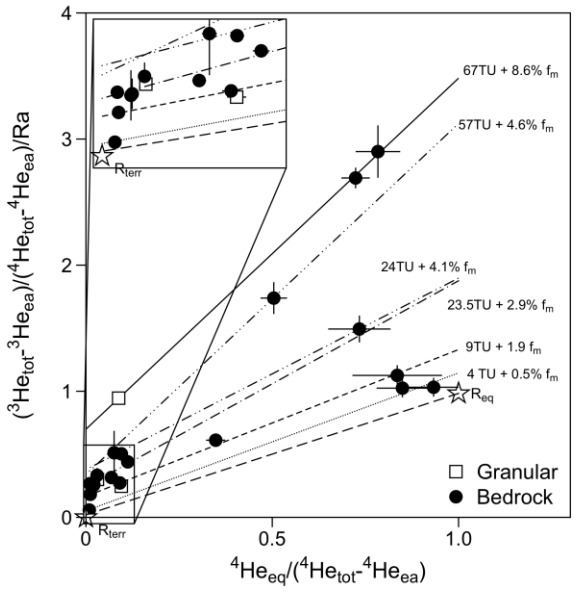

Saby et al. (2015)

Figure 5

Applied Geochemistry – To be submitted

a

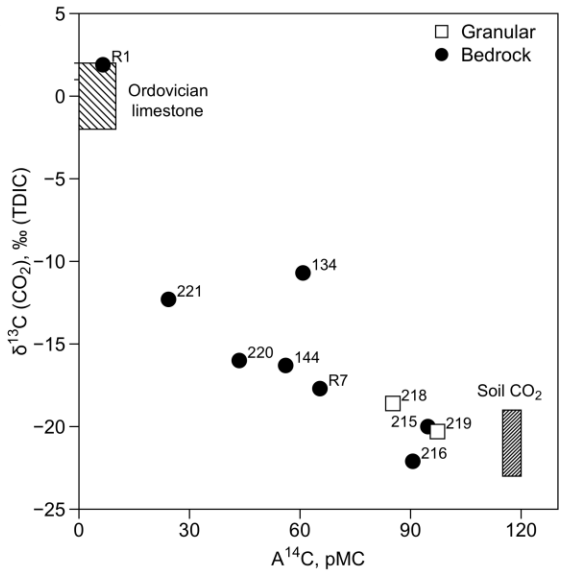

b

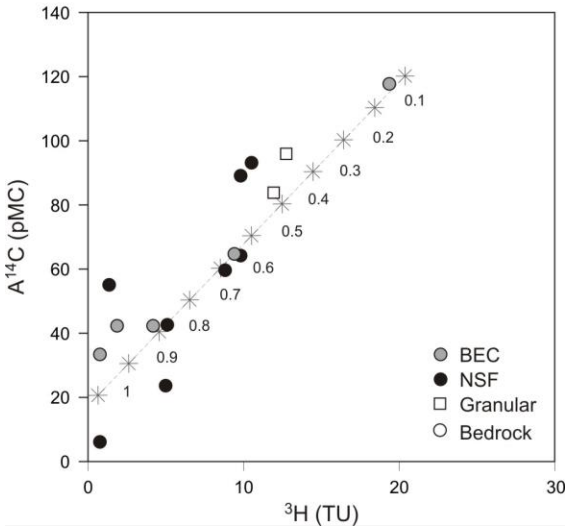

Saby et al. (2015)

Figure 6

Applied Geochemistry – To be submitted

a

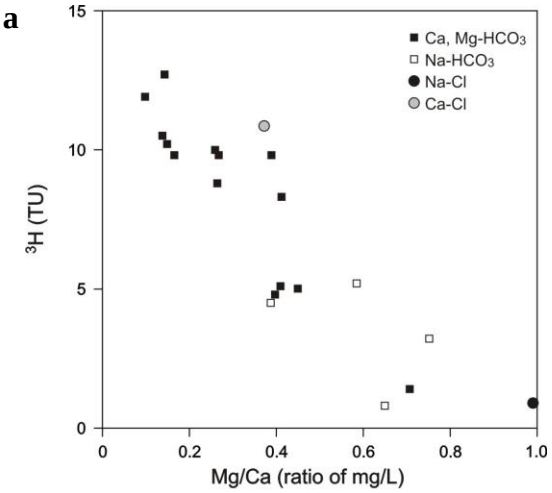
Ca, Mg-HCO3
Na-HCO3
Na-Cl
Ca-Cl
3H (TU)
Mg/Ca (ratio of mg/L)

b

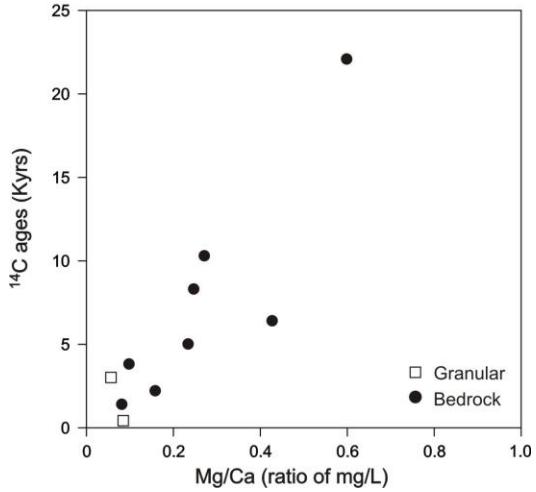
14C ages (Kyrs)
Granular
Bedrock
Mg/Ca (ratio of mg/L)

c

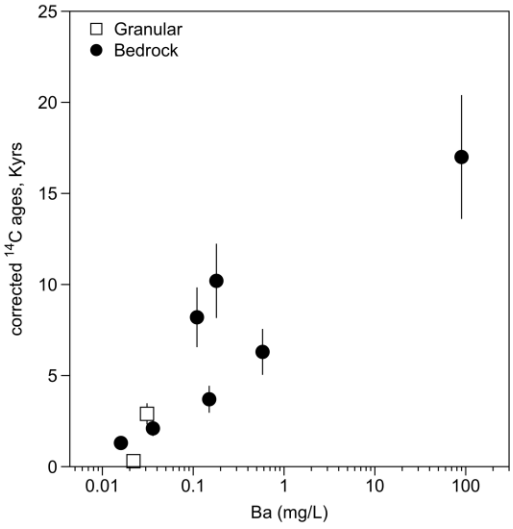
Granular
Bedrock
corrected 14C ages, Kyrs
Ba (mg/L)

Saby et al. (2015)

Figure 7

Applied Geochemistry – To be submitted

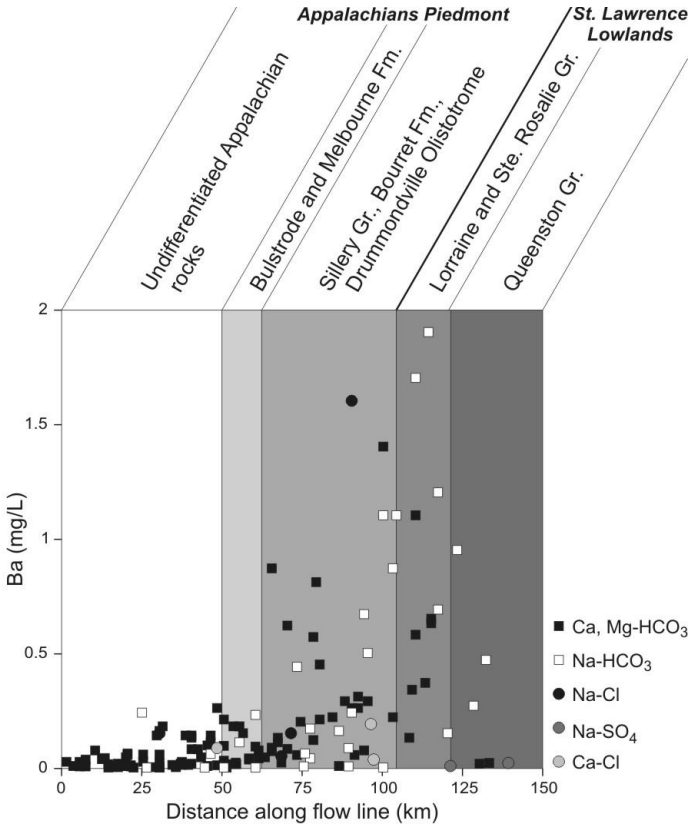

Saby et al. (2015)

Figure 8

Applied Geochemistry – To be submitted

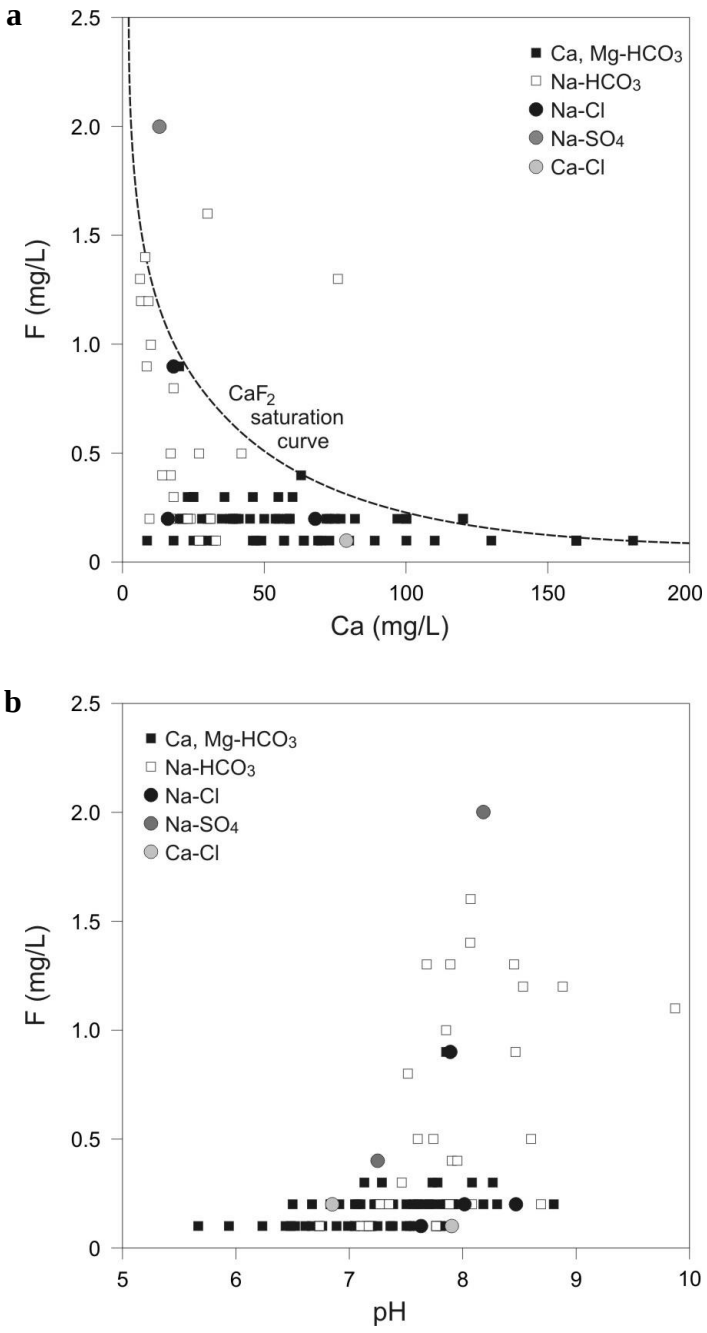

Saby et al. (2015)

Figure 9

Applied Geochemistry – To be submitted

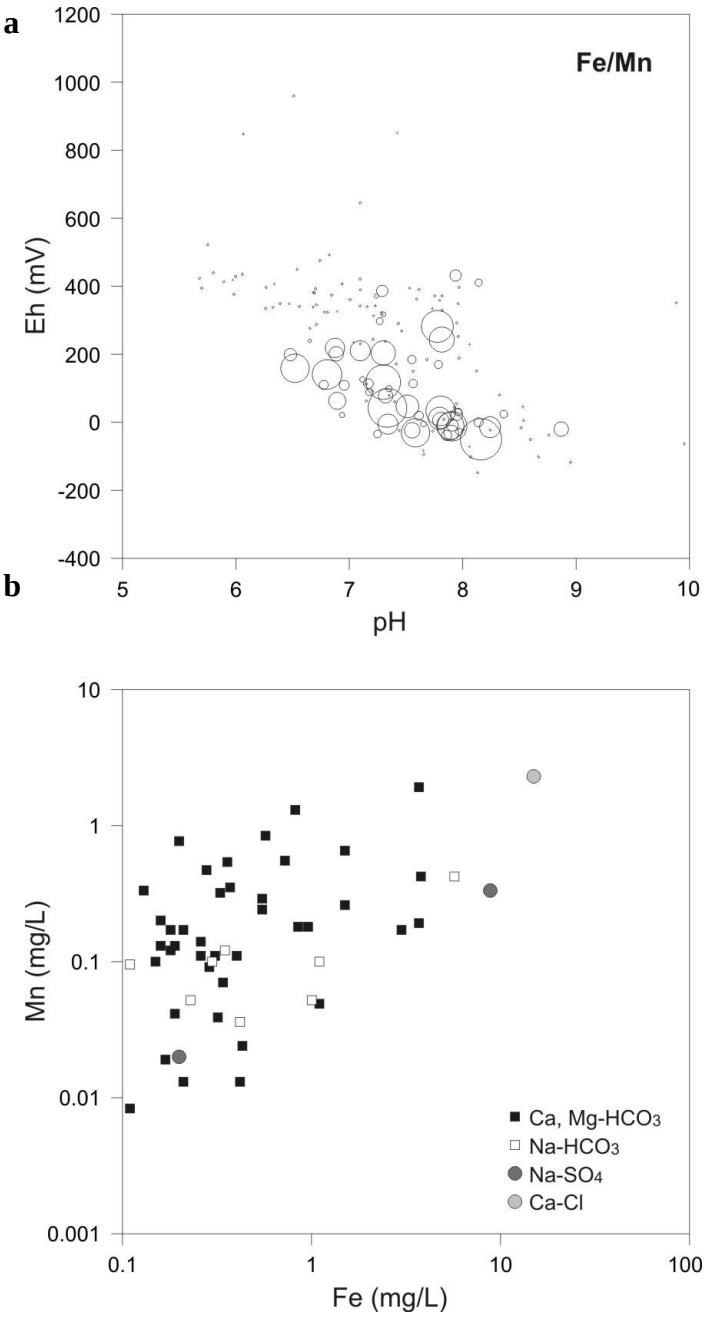

Saby et al. (2015)

Figure 10

Applied Geochemistry – To be submitted